Indonesian Journal on Geoscience Vol. 13 No. 3 December 2026: 373-392

INDONESIAN JOURNAL ON GEOSCIENCE
Geological Agency
Ministry of Energy and Mineral Resources

Journal homepage: https://ijog.geologi.esdm.go.id
ISSN 2355-9314, e-ISSN 2355-9306

Comprehensive Evaluation of Sandstone Reservoirs: A Methodological Study on The Impact of High Chlorite Content

Thanh Tung Nguyen, Hoang Anh Nguyen, Thuan Van Nguyen,
Triet Le Minh, and Quang Tuan Nguyen

Vietnam Petroleum Institute, 167 Trung Kinh, Cau Giay, Hanoi, Viet Nam

Corresponding author: anhnh@vpi.pvn.vn
Manuscript received: April 21, 2025; revised: July, 23, 2025;
approved: April, 29, 2026; available online: August 3, 2026

Abstract - Chlorite-bearing sandstone reservoirs often pose challenges in hydrocarbon zone interpretation due to their dual effects: porosity preservation and pore-throat blockage at depth. For a better understanding, this study integrates multiple methodologies, including mineralogical analysis of core samples and petrophysical logging, to classify and to assess the influence of high chlorite content on reservoir quality; a comprehensive well log interpretation approaches and machine learning (ML) to water saturation estimation in chlorite-affected intervals. Based on porosity and permeability measurements, thin-section analysis, X-ray diffraction (XRD), scanning electron microscopy (SEM), as well as special core analysis (SCAL), the morphologies of chlorite are mainly grain-coating, rosetted boxwork, and floccules. Furthermore, the reservoirs are classified into four groups according to chlorite impact levels. Classes 1 and 2 exhibit minimal chlorite influence, whereas classes 3 and 4 show a significant chlorite effect. Notably, class 4 demonstrates lower permeability than class 3, despite higher porosity and a stronger impact of chlorite due to pore-throat blockage by abundant chlorite floccules. Water saturation analysis reveals that in high-chlorite zones, the dual-water model provides more accurate results than Archie's equation, whereas in low-chlorite intervals, both methods yield comparable outcomes. Additionally, ML-based predictions using the state-of-the-art LightGBM tool on well-log data exhibit strong alignment with core analysis and empirical calculations, with R^2= 0.8804 and RMSE = 0.0572. These findings significantly enhance water saturation estimation in chlorite-impacted reservoirs and demonstrate broad applicability for assessing chlorite distribution in wells with limited core data or well log datasets.

Keywords: chlorite, machine learning, well log, porosity, permeability, water saturation

How to cite this article:
Nguyen, T.T., Nguyen, H.A., Nguyen, T.V., Minh, T.L., Nguyen,Q.T., 2026. Comprehensive Evaluation of Sandstone Reservoirs: A Methodological Study on The Impact of High Chlorite Content. *Indonesian Journal on Geoscience*, 13 (3), p.373-392. DOI: 10.17014/ijog.13.3.373-392

Introduction

Background

Chlorite, an ubiquitous phyllosilicate mineral, plays a crucial role in numerous sedimentary and diagenetic processes, yet its significance has often been overlooked in previous mineralogical and geological studies (King, 2019). Moreover, chlorite, which is a clay mineral formed commonly through the weathering of silicate rocks, is an important component in the transportation of weathering products from continents to the sea (Gingele *et al.*, 2001). Sources of sediment in the hinterland are rich in mafic and metamorphic rocks (commonly containing minerals like biotite, amphibole, and pyroxene), resulting in a higher initial potential for chlorite formation because chlorite often forms from the alteration of these primary ferromagnesian minerals during transport (Mazumder, 2016). Chlorite is a group of iron- and magnesium-rich phyllosilicate minerals that commonly occur in low-temperature diagenetic environments and low-grade prograde metamorphic rocks (Deer *et al.*, 2013).

As an authigenic clay, chlorite commonly forms coatings around detrital quartz grains in sandstones, playing a crucial role in reservoir diagenesis. By inhibiting the precipitation of quartz overgrowths, chlorite helps preserve primary porosity and maintain favourable reservoir characteristics with high porosity and permeability, unlike those lacking the coating even at significant burial depths (Anjos *et al.*, 1999; Jia *et al.*, 2018; Li *et al.*, 2021). In complex reservoirs, conventional log interpretation may fail to account for clay-related surface conductivity, leading to overestimation of water saturation (Sw) when empirical models such as Archie's equation and the Dual-Water model are applied without mineralogical constraints (Archie, 2003; Clavier *et al.*, 2003). Traditionally, Sw is determined through direct laboratory analysis of core samples and indirect calculations using empirical equations with well log data. Archie's equation is widely used for water saturation estimation but is mainly applicable to clean sandstones, whereas the Dual-Water model accounts for both bound and free water components (Durand *et al.*, 2000; Hamada and Al-Awad, 2000).

An alternative approach to estimating the irreducible water saturation (Swi) is through capillary pressure (Pc) measurements, which provide a more detailed understanding of fluid distribution and rock wettability (Brooks and Corey, 1964; Leverett, 1941). Pc-based Swi determination is particularly useful in formations where core extraction is limited, enabling more reliable calibration of log-derived water saturation. By integrating Pc-derived Swi into empirical saturation models, uncertainties in Sw estimation can be significantly reduced, thereby improving reservoir characterization in chlorite-rich sandstone formations (Tiab and Donaldson, 2015). Nevertheless, core analysis is expensive, time-consuming, and provides only discrete data points that may not be fully representative of the entire reservoir. Moreover, despite their high accuracy, core data are usually unavailable for all wells in a field, whereas well logs are routinely acquired in most wells.

Recently, there has been a lot of interest in the application of machine learning (ML) in the geosciences because of its enormous potential (Bukar *et al.*, 2019; Hadavimoghaddam *et al.*, 2021; Hu *et al.*, 2023; Mollajan and Memarian, 2013; Saumya *et al.*, 2019). Well log correction, normalization, logging service optimization, petrophysical property prediction, and laboratory measurement cost reduction are all made possible by machine learning approaches. Consequently, many studies have been conducted by the use of ML methods in well log interpretation (Shao *et al.*, 2019), prediction of sonic logs (Bukar *et al.*, 2019), reservoir characterization such as porosity and permeability as well as lithology (Hu *et al.*, 2023), water saturation. Among the machine learning methods used recently, Light Gradient Boosting Machine (LightGBM), which is the state-of-the-art algorithm based on gradient boosting trees, is widely used in data science for achieving significant results such as lithology identification, reservoir permeability and porosity (Friedman, 2001; Shao *et al.*, 2019).

Previous studies in The Nam Con Son Basin have rarely quantified the direct impact of chlorite on both reservoir quality and water saturation using integrated mineralogical and petrophysical datasets. Moreover, the application of machine learning to investigate chlorite-controlled Sw behaviour remains limited. To address the above problems, this study primarily aims to conduct a comprehensive investigation into the distribution and effect of authigenic chlorite by classifying its effect on reservoir properties. This classification is based on detailed core data analysis and conventional well logs, including neutron-density, sonic, and resistivity logs. Furthermore, the study integrates core-derived information with petrophysical data to assess the applicability of water saturation estimation models in chlorite-rich intervals. Specifically, it examines whether the clean sand model (Archie's equation) or the shaly-sand model (Dual-Water equation) provides more accurate Sw estimations in formations with high chlorite influence. Additionally, this research employs machine learning techniques, particularly LightGBM-based predictive modeling, to enhance Sw estimation and chlorite effect investigation in the SA Oil Field. By leveraging ML algorithms alongside traditional petrophysical models, this study aims to improve water saturation predictions in complex reservoirs, ultimately enhancing hydrocarbon potential assessment and reservoir characterization.

Geological Setting

The studied area, SA Field, is located in the southeastern section of the Nam Con Son Basin, offshore Vietnam (Figure 1) and approximately 350 km SE of Vung Tau. It is a three-way dip-closed structure, relying on an updip fault located directly southwest. Previous studies from Tuan *et al.* (2016) and Tung (2015) are elaborated for the detail of tectonic and stratigraphic developments of SA Field and NCSB.

The tectonic evolution of The Nam Con Son Basin was controlled by multiple rifting and extensional phases from The Eocene to Miocene, with initial rifting in The Eocene-Early Oligocene characterized by N-S extension and E-W-orientated fault systems, followed by a second extensional phase in the early Miocene associated with the opening of The East Sea and the development of NE-SW-trending normal faults and sediment-filled grabens (Tuan *et al.*, 2016). This rifting period was then followed by the deposition of a thick post-rift sedimentary sequence (Upper Miocene to Quaternary) due to increased sediment input from onshore uplift and magmatism (Fyhn *et al.*, 2009; Hall and Spakman, 2015; Tung, 2015).

The main reservoirs in SA Field, including Zone 1 (Z1) and Zone 2 (Z2), correspond to The Lower Miocene Middle Dua Sandstone at depths of approximately 3,500 m TVDSS (Figure 1c). These reservoirs are characterized by vertically stacked sandstone-shale successions, with reservoir-quality sand bodies typically capped by shale layers. Deposition is interpreted to have occurred in a marginal marine to nearshore, tide-dominated environment, where erosive-based sand bodies overlie prodelta shales and evolve upward into heterolithic facies. The reservoir succession overlies The Cau Formation across a regional unconformity, with basal transgressive sandstones marking the base of The Dua Formation (Duyen *et al.*, 2023; Tuan *et al.*, 2016).

Methods and Materials

A total of 81 m and 115 m of sandstone cores from the Z1 and Z2 reservoirs, respectively, were available from three wells (Well 1, Well 2, and Well 3) in The SA Field. These cores were analyzed using X-ray diffraction (XRD), scanning electron microscopy (SEM), thin section petrography, routine core analysis (RCA), and special core analysis (SCAL).

Conventional petrographic analysis was performed on eighty-nine thin sections from sandstone reservoir cores to characterize mineral composition and diagenetic features. Scanning electron microscopy (SEM) was applied to twenty-five chlorite-rich samples to investigate chlorite morphology and petrographic relationships. X-ray diffraction (XRD) analysis was conducted on twenty representative samples to identify and quantify clay mineral assemblages, including chlorite. Routine core analysis (RCA) was carried out on 727 samples to measure porosity and permeability, while special core analysis (SCAL) was performed on thirty-eight samples from three wells to estimate water saturation.

All petrographic, SEM, XRD, and SCAL data used in this study were obtained from certified laboratory reports provided by Oolithica Geoscience Ltd. (UK). These analyses were performed following standard industry procedures using

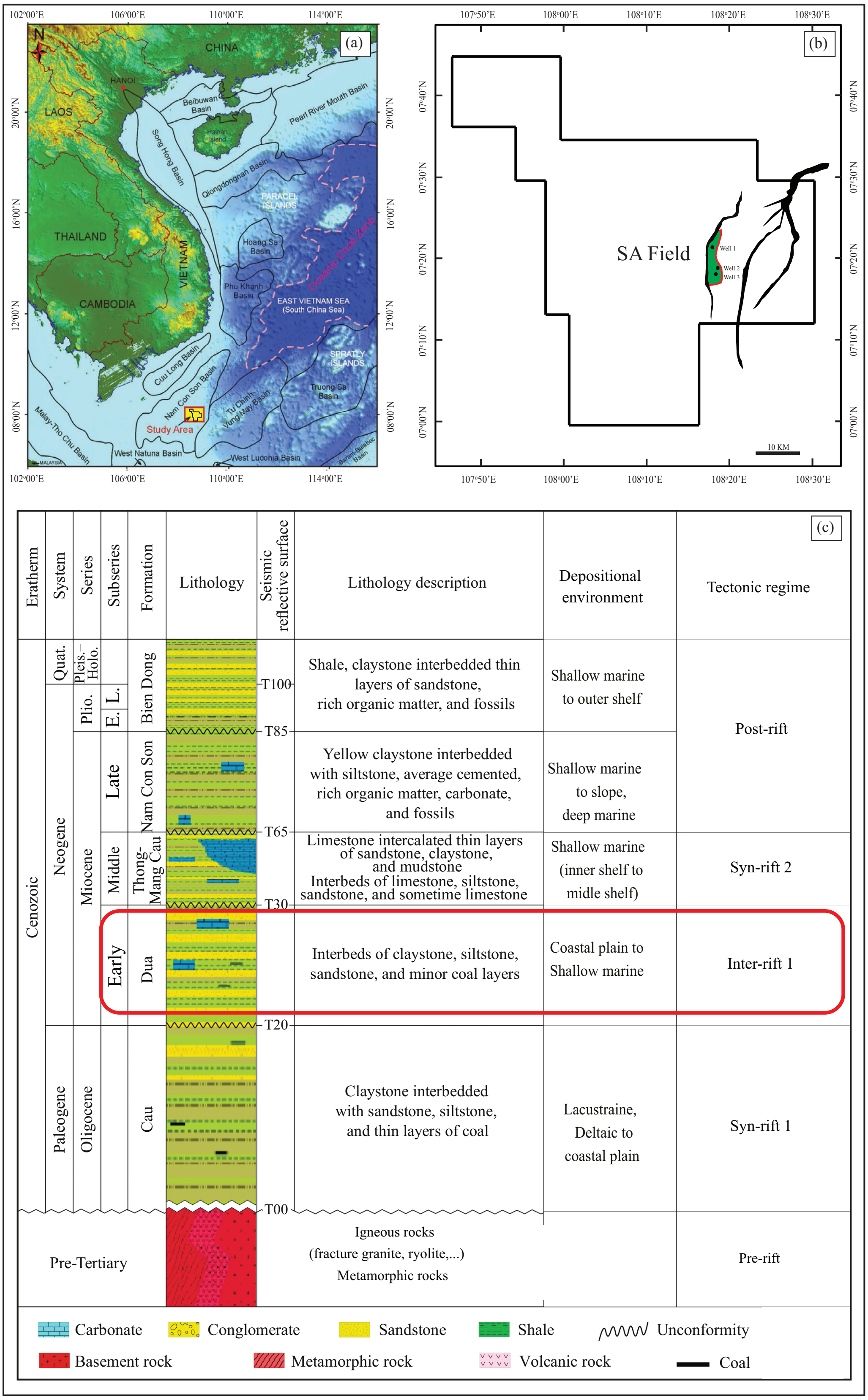

Figure 1. (a). Overview of the studied area, which is located in the SA Field, Nam Con Son Basin, offshore Vietnam; (b) Map showing the studied wells in the studied area with a three-way dip-closed structure, relying on updip; (c) Chronostratigraphic chart of Tertiary sediments with the studied formation (red box) in the SA Field (modified from Duyen *et al*., 2023; Tuan *et al*., 2016).

calibrated instruments. The datasets were supplied to the authors by PetroVietnam and were used for subsequent reservoir property analysis and petrophysical interpretation.

The suite of petrophysical logs were taken from these three wells, such as Gamma Ray (GR), Neutron (NPHI), Bulk Density (RHOB), Deep Resistivity (LLD), and Sonic (DTCO) was used to interpret the shale volume, porosity and water saturation as well as to analyze cross-correlations among log responses for identifying chlorite effects. All log processing and interpretation were performed using Techlog software (Schlumberger). The shale volume was calculated by using both GR and combined NPHI-RHOB methods and constrained with XRD data to minimize uncertainties. Porosity was estimated from the NPHI-RHOB combination equation (Asquith and Gibson, 1982), and calibrated with measured porosity from RCA. Water saturation was calculated by using both Archie's equation (Archie, 2003) and the Dual-water (DW) model, which accounts for clay-bound water effects in shaly sandstones (Clavier *et al.*, 2003) with parameters of tortuosity factor (a) = 1, cementation exponent (n) = 1.98, and saturation exponent (m) = 1.92. The calculated water saturation results were validated against SCAL-derived measurements from thirty-eight core samples across the three wells.

Petrophysical well log curves such as GR, NPHI, RHOB, LLD, and DTCO as well as calculated porosity and Sw from Well 1 and Well 2 are ultimately used as inputs to build a model for Sw prediction, while Well 3 was reserved for blind testing. Light Gradient Boosting Machine (LightGBM), a fast and efficient machine learning algorithm based on the gradient boosting decision trees and developed by Microsoft Research Asia in 2016 (Machado *et al.*, 2017) was applied for model building. Model performance was evaluated using coefficient of determination (R^2), which indicates the proportion of variance explained, and the root mean squared error (RMSE), which quantifies the average prediction error.

Results

Spatial Distribution of Chlorite in Z1 And Z2 Reservoirs

The sandstones of the Z1 and Z2 reservoirs in three wells in SA Field exhibit compositional variation as depicted on a Quartz (Q), Feldspar (F), and Lithic Fragments (L) ternary diagram (Figure 2). Well 1 samples, represented by a circle, are primarily litharenites with an average framework composition of $Q_{48}F_3L_{49,}$ which comprises quartz ranging from 40.7 % to 57.5 % with an average of 47.9 %; feldspar grains accounting for 0.1-7.3 % with an average of 3.2 %; as well as lithic comprising 39.8-58.2 % with an average of 48.9 %. Meanwhile, Well 2 and Well 3 display less variability and trend more towards the quartz-rich and less lithics, which are predominantly within the litharenite and feldspathic litharenite. Based on point-counting data, detrital feldspar is the least dominant grain (5.2-18.2 %, average 10 %), whereas the detrital quartz is the most abundant grains, ranging from 45.9-67.8 % (average 58 %). Lithic fragments make up 21.5-40.6 % (av.32 %). Therefore, the average composition is approximately $Q_{58}F_{10}L_{32}$.

The mineral composition of sandstone samples was analyzed using X-ray diffraction (XRD) patterns. This technique provides quantitative data on the proportions of crystalline minerals,

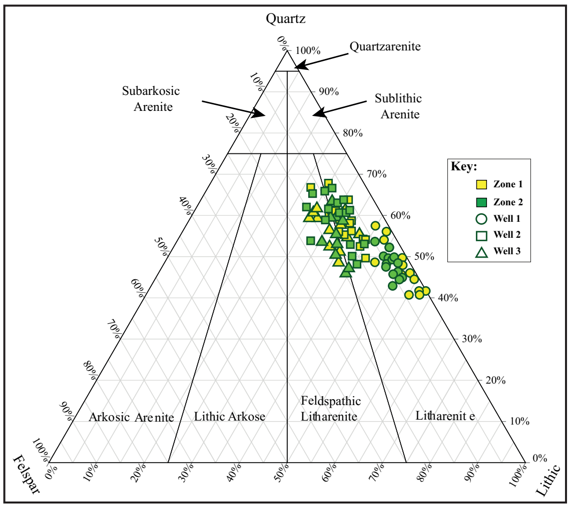

Figure 2. Rock classification of sandstone reservoirs based on Folk's (1974) criteria in SA Field.

which is useful for understanding petrophysical properties such as mineral identification and quantification; this, in turn, helps determine clay volume, clay/silt ratio, and rock type, thereby justifying the selection of appropriate well-log interpretation models. In this study, the samples came from depths between 3,600 m and 3,900 m. Results showed that the Z1 and Z2 sandstone reservoirs in the SA Field are primarily composed of quartz, illite, chlorite, plagioclase, and K-feldspar (Figure 3a). The abundance of these minerals varied considerably among the samples. Quartz is the most abundant mineral, ranging from about 67% (Z1 in Well 1) to 80% (Z2 in Well 3). The second dominant composition in this area is illite, which is distributed between 5.5% (Z2 in Well 3) and 10.3% (Z1 in Well 1). In addition, the chlorite content varies from 3.5% to 7% and has the highest average amount in the Z1 reservoir in Well 1. Moreover, other mineral components such as siderite, pyrite, calcite, chamosite, and glauconite appear as a trace or less than 4 % for each. On the other hand, minor bioclasts include intraclasts and mudclasts, also observed in this area.

XRD analyses for the clay fraction (< 2µm) indicate that chlorite, accounting for more than 68 % of total clay minerals and ranging from about 65 % to 85 % (Figure 4b) is the dominant clay mineral compared to brittle minerals (like quartz). Mixed-layer illite/smectite is only found in Well 1 with low content (5-7%), while illite is also discovered as a secondarily abundant element in clay minerals with content from 16% to 24% (Figure 4a). Other minerals, like siderite or calcite, are present only as traces in clay minerals.

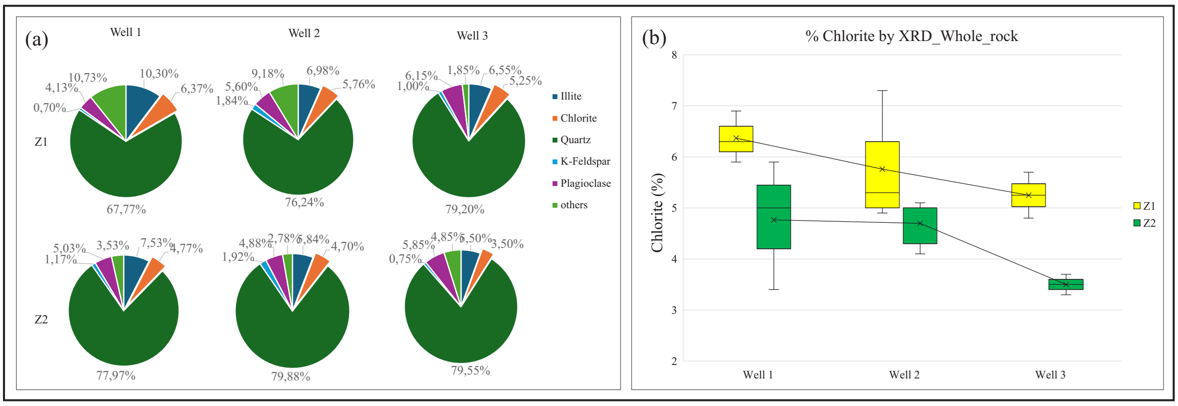

Figure 3. (a). XRD Whole rock in SA Field. The average percent of chlorite (orange colour) among whole rock mineralogy; (b). Distribution of chlorite amount in Z1 and Z2 reservoirs in three wells, SA Field.

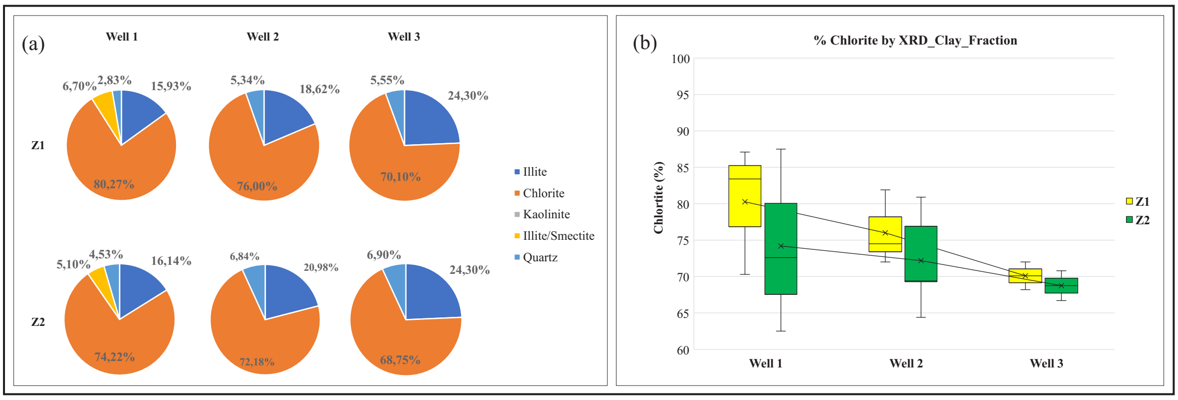

Figure 4. (a). XRD Clay fraction in SA Field. The average percent of chlorite (orange colour) among authigenic clays; (b). Variety of chlorite amounts within authigenic clay minerals in Z1 and Z2 reservoirs of three wells, SA Field.

Classification of Chlorite Levels in SA Field

The aim is to establish a petrophysically manageable number of sedimentary facies based on their petrophysical associations and prevalence derived from available core data in the Z1 and Z2 reservoirs of three wells in the SA Field. Chlorite classes were defined using an integrated, multicriteria approach that combines (i) clustering domains on porosity-permeability cross-plots, (ii) chlorite textural occurrence (pellicles versus floccules) observed from thin section and SEM analyses, and (iii) diagnostic core-based depositional facies attributes with the same class signatures observed across both Z1 and Z2 reservoirs.

This classification suggests that reservoir properties can be grouped into four principal porosity-permeability (poroperm) classes (Table 1, Figures 5a-g, and Figures 6a-e), based on core-derived parameters including grain size, mud content, bedding style (*e.g.* lenticular, wavy, or flaser), degree of bioturbation, and sediment composition. Poroperm Classes 1 and 2 represent the normal reservoir trend for the Z1 and Z2 intervals, whereas Classes 3 and 4, despite similar sandstone lithologies, are primarily associated with progressively stronger diagenetic chlorite effects. Overall, chlorite influence decreases from Z1 to Z2 and from Well 1 to Well 3. Class 4 occurs exclusively in the Z1 reservoir of Well 1 and is associated with the highest porosity. Class 3 is also more prevalent in Z1 than in Z2, whereas Class 1 and Class 2 dominate in Z2 and become increasingly common toward the southern part of the SA Field.

Class 1 clustered in the lower-left region of the cross-plot in Figure 5 and Figure 6a: variable/fractured plugs or rare-chlorite effect with mostly mud-dominated lithofacies and intraformational conglomeratic lags. These plugs have a widespread occurrence due to their micro-heterogeneous nature and propensity to fracture during core analysis. Class 1 in the core image consists of lenticular bedded very fine-fine-grained heterolithic sandstone and mudstone which are climbing sigmoidal ripples, separated by mud drapes, as well as wave-rippled sand lenses.

Class 2 in the central region of the cross-plot of Figure 5 and displays thin chlorite pellicles forming discontinuous grain coatings in Figure 5b. Normal reservoir trend or low chlorite effect controlled largely by increasing grain size/decreasing mud content. Sand typically exhibits

Table 1. Summary of chlorite-controlled porosity and permeability classes

Class	Poroperm domain	Chlorite level / type	Core facies (core image / sedimentary features)	Petrographic and SEM characteristics
1	Low-Φ / low-K domain (Fig. 5, 6a)	Rare or negligible chlorite	Mud-dominated heterolithic facies; lenticular and flaser bedding; sigmoidal ripples; intraformational conglomeratic lags	Mud-rich micro-heterogeneous fabrics; mechanical fracturing common; negligible chlorite
2	Moderate-Φ / moderate-K domain (Fig. 5, 6b)	Thin, discontinuous pellicles	Cross-bedded fine–medium sandstone; minor mud flasers; mud-draped toesets	Thin chlorite coatings; abundant quartz overgrowth; partial leaching
3	High-Φ / variable-K domain (Fig. 5, 6c–d)	Thick, continuous pellicles; minor floccules near pore throats	Well sorted very fine–fine sandstone; ripple and tidal cross-lamination; herringbone structures	Multiple generations of chlorite pellicles lining pores; strong inhibition of quartz cement; minor floccules near throats
4	High-Φ / low-K domain (Fig. 5, 6e)	Abundant floccules densely at pore throats; rosetted overgrowths	Fine-grained massive-bedded sandstone	Dense floccules and rosetted chlorite crystals plugging pore throats; intraparticle microporosity dominant

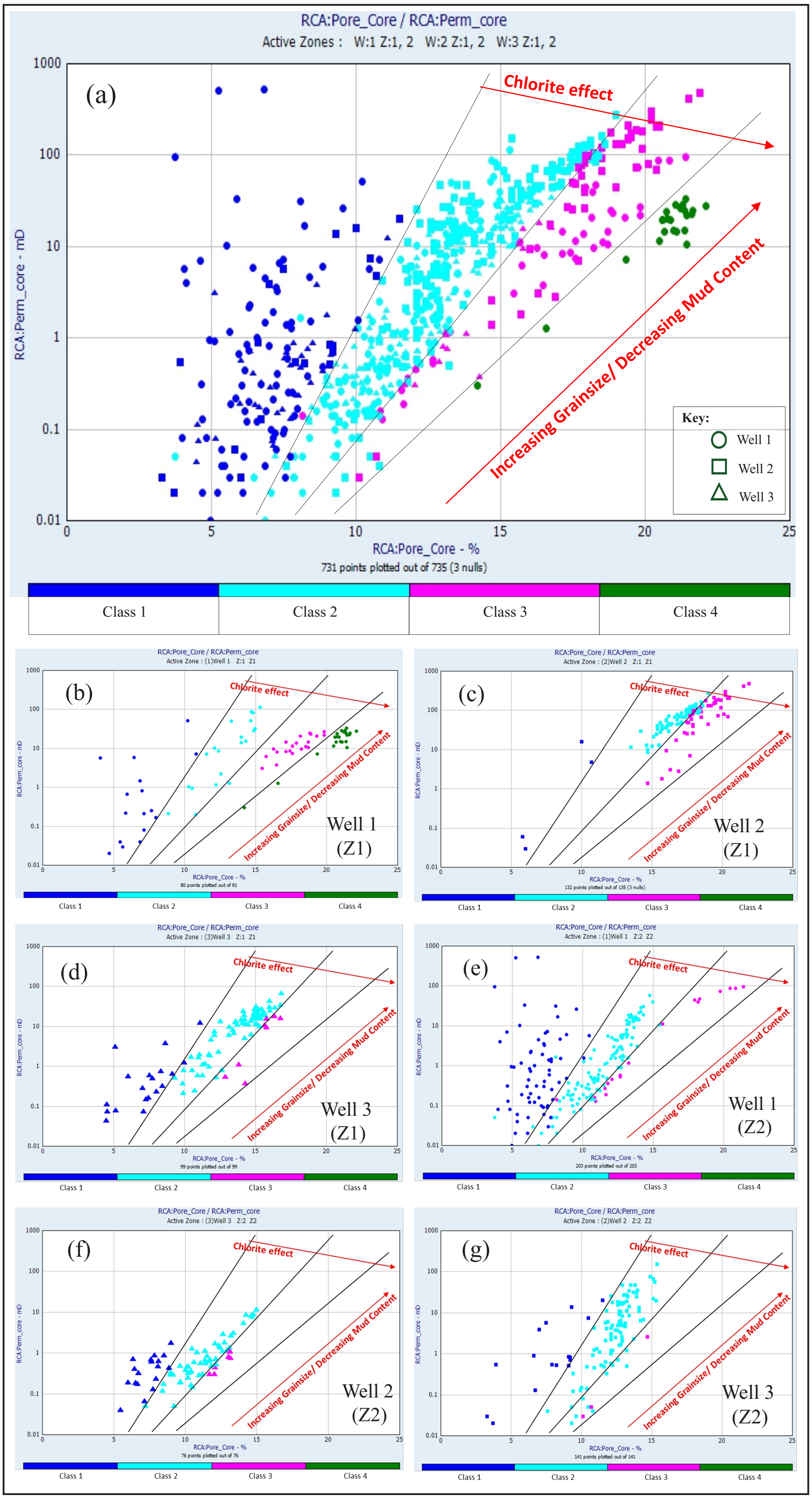

Figure 5. (a). Classification of chlorite effect based on RCA (porosity permeability) from three wells in SA Field where is Class 1 (blue): none-effect, Class 2 (cyan): normal sandstone - minor effect, Class 3 (fuchsia): moderate effect, Class 4 (green): strong effect; (b - g). Classification through wells and reservoirs.

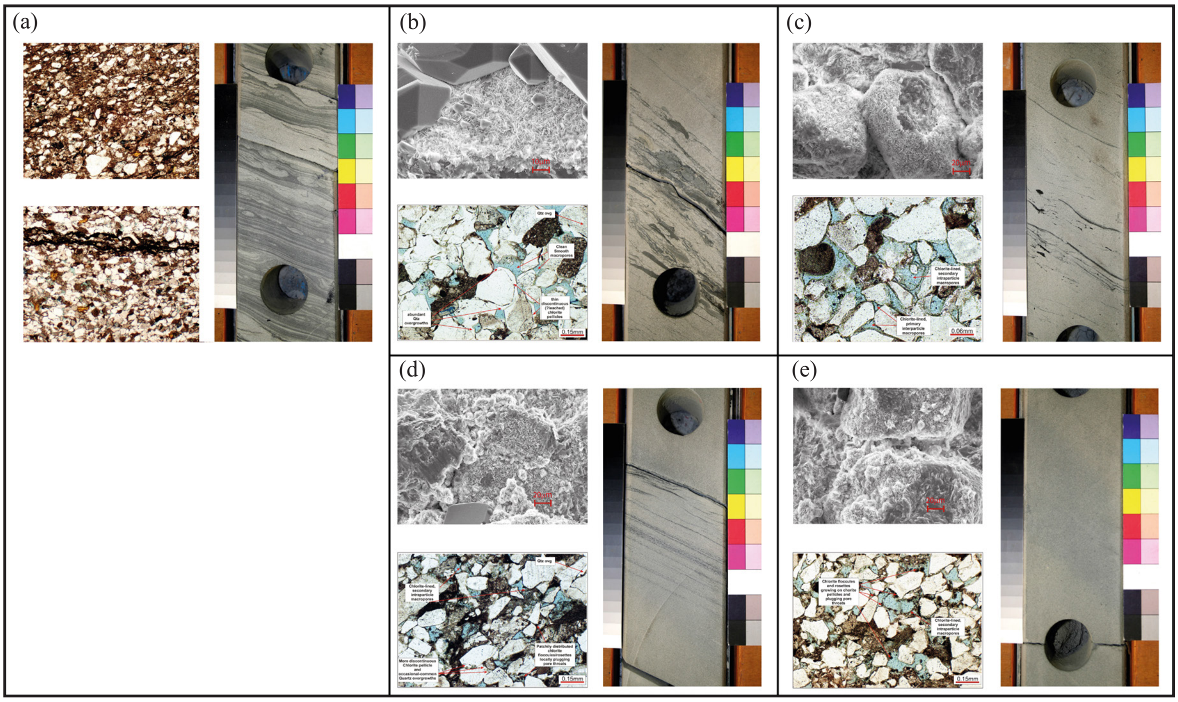

Figure 6. Representation of thin section and SEM as well as core image for each class in poro-perm data. (a) CLASS 1: A very fine lithic arenite and clay-rich, with no visible porosity and tight as well as no chlorite. (b) CLASS 2: thin chlorite pellicles, discontinuous grain coatings, no chlorite floccules and rosettes at pore throats, and common-abundant quartz overgrowths. (c) CLASS 3: with high permeability: thick chlorite pellicles, continuous grain coatings. No chlorite floccules and rosettes and negligible quartz overgrowths. (d) CLASS 3: with reduced permeability: Moderate chlorite floccules with later crystalline rosetted overgrowths plug pore throats with reduced permeability. (e) CLASS 4: Fine-grained lithic arenite. Thick chlorite pellicles, fairly continuous grain coatings, and abundant chlorite floccules and rosettes at pore throats result in impaired permeability.

thin chlorite grain coating and moderate quartz overgrowth. Moreover, this trend is common to Z1 and Z2 reservoirs, where chlorite lines the pore but does not fully inhibit quartz overgrowth. In class 2, it shows cross-bedded fine- to medium grained moderately well sorted sandstone with minor mud flasers, and mud draped toesets. In thin section, chlorite displays thin or discontinuous pellicles with resultant abundant quartz overgrowths, leaching of chlorite pellicles and framework grains also occurred.

Class 3 (Figure 5 and Figure 6c): moderate chlorite effect corresponds to high porosity ranging from 10-20% and permeability associated with heavy chlorite grain-coating with wide ranges (1-500mD), greatly reducing quartz overgrowth and lack of chlorite floccules at pore throats, resulting in maintaining permeability. These increase microporosity and preserve higher levels of intergranular porosity through inhibiting quartz overgrowth. Although the class 3 keeps maintaining the high porosity, permeability has also been reduced due to heavy chlorite cements and minor chlorite floccules concentrating near pore throats (Figure 5 and Figure 6d). Furthermore, for class 3 (Figures 6c-d), the core image presents very fine - fine-grained and moderately well-to-well sorted, with a variety of small, medium and rarely large-scale cross-bedding. In addition, various types of ripple lamination are present, ranging from current wave to combined flow, with herringbone tidal structures present. Representative thin section in class 3 (Figure 6c) shows that multiple generations of chlorite pellicles are dominant, resulting in widespread, thick, continuous lining of pores which has strongly inhibited quartz overgrowths and preserved primary porosity. Thus, there are very good secondary and primary microporosity. However, there are moderate chlorite floccules with later crystalline rosetted overgrowths plugging pore throats and more patchily distributed than in class 4 resulting in reduced permeability (Figure 6d).

Class 4 (Figure 5 and Figure 6e) corresponds to a strong chlorite effect with heavy chlorite development, especially as chlorite floccules occur at pore throats, systematically impairing permeability but preserving porosity through greatly reduced quartz overgrowth. The core image of class 4 shows that sandstone has fine grain and appears massive bedding with elevating chlorite levels. Figure 6e shows that the abundant floccules-like chlorite movably and densely plugs in pore throats and later crystalline rosetted overgrowths. This class 4 also exhibits very good porosity and is dominant with intraparticle microporosity.

Well-log Recognition of Chlorite-cemented Sandstone Reservoirs And Petrophysical Interpretation Results

Log and core data from the chlorite-cemented Z1 and Z2 sandstone reservoirs in the SA Field, Nam Con Son Basin, are presented in Figures 7-9. Figures 7a-h show the relationships between RCA-derived porosity and conventional well logs (RHOB, NPHI, LLD, and DTCO) for different chlorite classes (Classes 1-4). The four classes are clearly separated in all cross-plots. DTCO and NPHI systematically increase with increasing chlorite effects, whereas RHOB and LLD decrease. Class 4, representing the strongest chlorite influence, occurs mainly in the Z1 reservoir and exhibits the highest porosity (>20%), lowest density (<2.42 g/cm³), highest DTCO (>80 µs/ft), and lowest resistivity. Class 3 shows a moderate chlorite effect with a porosity of ~17-20% and a DTCO of 75-80 µs/ft, while Class 1 and Class 2, corresponding to weak or negligible chlorite influence, display lower porosity (<17% and <10%, respectively) and higher density and resistivity.

Conventional well logs show clear mineralogical signatures across the three wells, enabling cross-plots to evaluate chlorite effects (Figure 8). NPHI-RHOB cross-plots indicate that chlorite influence decreases southward from Well 1 to Well 3, with chlorite-rich classes characterized by higher NPHI (>0.15) and lower RHOB (<2.42 g/cm³). Deep resistivity–sonic cross-plots further confirm this trend, showing decreasing LLD with increasing chlorite content, particularly in Well 1, where Class 3 and Class 4 exhibit resistivity values of 5-8 Ohm·m and <5 Ohm·m, respectively. Resistivity displays higher variability than other logs, reflecting the combined effects of chlorite and hydrocarbon presence.

Well-log-derived water saturation using the Archie and Dual-Water equations is shown in Track 9 of Figure 9 and calibrated against core analysis results. The Dual-Water model shows good agreement with core-derived Sw, indicating its suitability for chlorite-rich intervals, whereas the Archie-derived Sw systematically overestimates water saturation in Z1 and Z2 reservoirs, particularly in high-chlorite classes (Classes 3 and 4) of Well 1. Toward the southern SA Field (Wells 2 and 3), where chlorite influence is weaker and reservoirs are mainly classified as Class 1 and Class 2, the results from Archie and Dual-Water equations become more comparable. Shale volume (Track 4) calculated from GR and combined RHOB–NPHI methods shows excellent consistency with XRD results. Porosity derived from RHOB–NPHI (Track 8) correlates well with RCA data and generally decreases with burial depth, with higher porosity in Z1 than in Z2, except in Well 3, where porosity remains similar in both reservoirs.

Machine Learning-based Water Saturation Prediction

The ML model was trained using data from Well 1 and Well 2 and then applied to predict water saturation in Well 3. The predicted Sw shows good agreement with both core-derived Sw and Dual-Water-based Sw (track 9 of Figure 9 in Well 3), while the difference between Archie and Dual-Water models is less significant in Well 3 due to weaker chlorite influence. Model performance was evaluated using R^2 and RMSE (Figure 10, Table 2). The R^2 value between ML

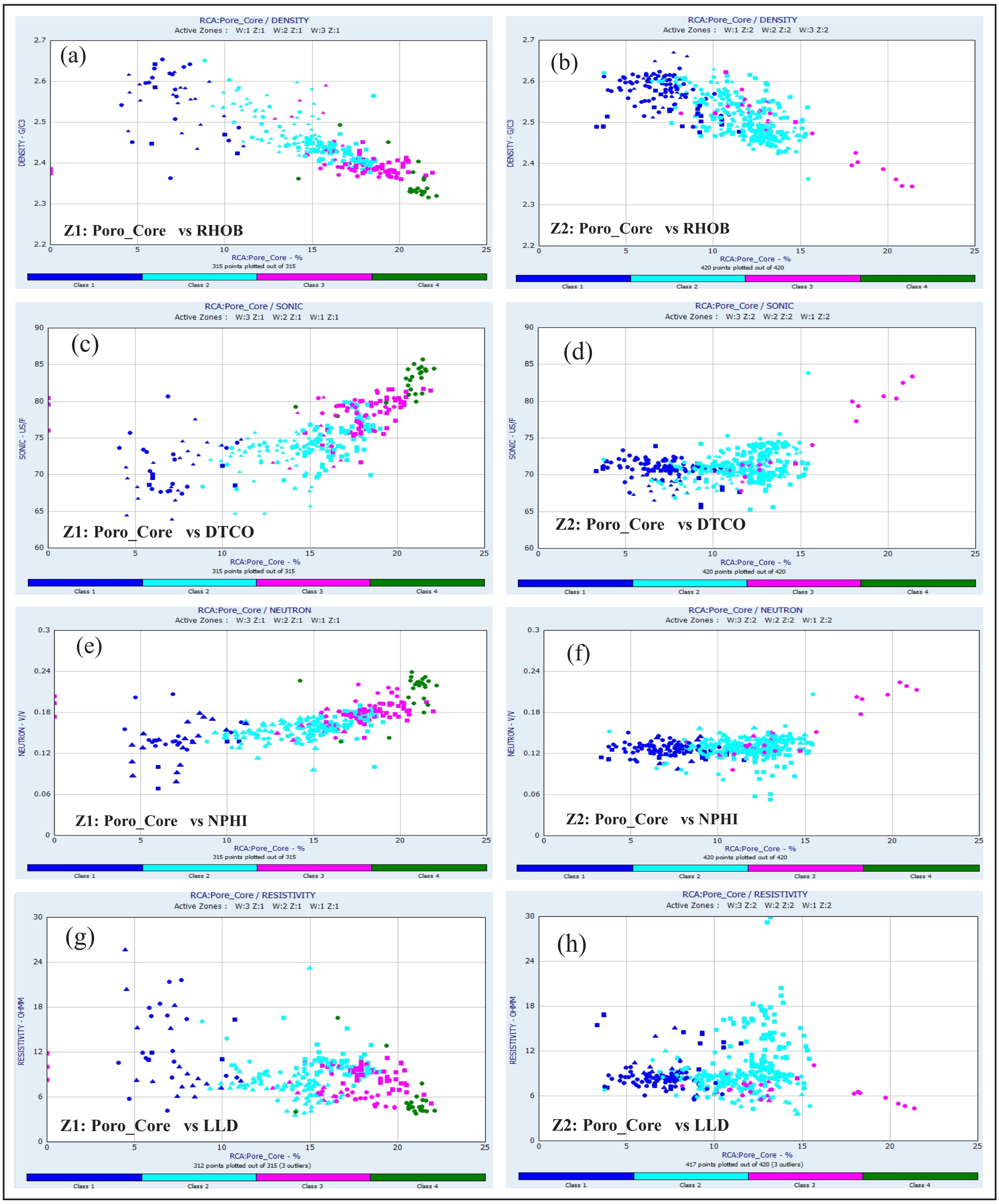

Figure 7. Representative well log responses of different classes of chlorite-bearing Z1 and Z2 reservoirs against porosity core data in Well 1 (circle), Well 2 (square) and Well 3 (triangle); (a, b) core porosity versus bulk density; (c, d) core porosity versus compressional sonic; (e, f) core porosity versus neutron; (g, h) core porosity versus deep resistivity.

prediction and the Dual-Water model is higher (0.881) than that with Archie's equation (0.783), indicating stronger consistency with the DW approach. RMSE values further confirm this result, with lower error for ML vs. Dual-Water (RMSE = 0.057) compared to ML vs. Archie (RMSE = 0.086). Overall, the ML model demonstrates reliable performance for Sw prediction and shows closer agreement with the Dual-Water model, particularly in chlorite-affected reservoirs.

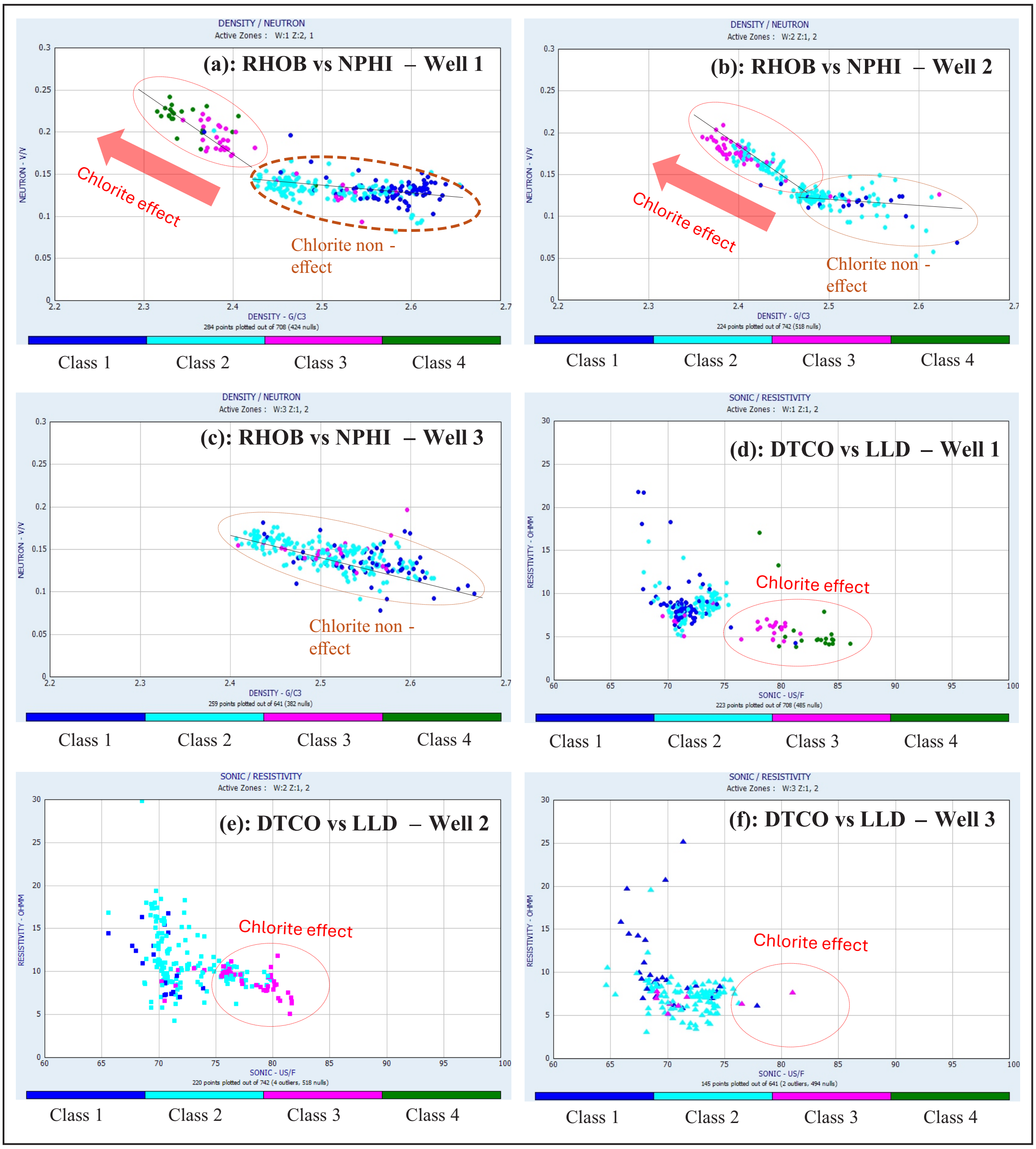

Figure 8. Cross-plots of neutron (NPHI) - density (RHOB) and sonic (DTCO) - deep resistivity (LLD) from representative well data were extracted at depth analyzed RCA in three wells.

Discussion

Diagenesis And Effect of Chlorite on Reservoir Quality

A key observation from this study is the distinct north-to-south decreasing trend in chlorite distribution within The SA Field, as illustrated in Figures 3 and 4. Well 1 exhibits significantly higher chlorite content, associated with more mineralogically immature to submature litharenitic sandstones, indicating favourable conditions for extensive chlorite development during early diagenesis. In contrast, Wells 2 and 3 show similar sediment compositions dominated by immature litharenites and feldspathic litharenites, with relatively lower chlorite abundance, suggesting weaker chlorite cementation and reduced diagenetic impact on reservoir quality. The observed

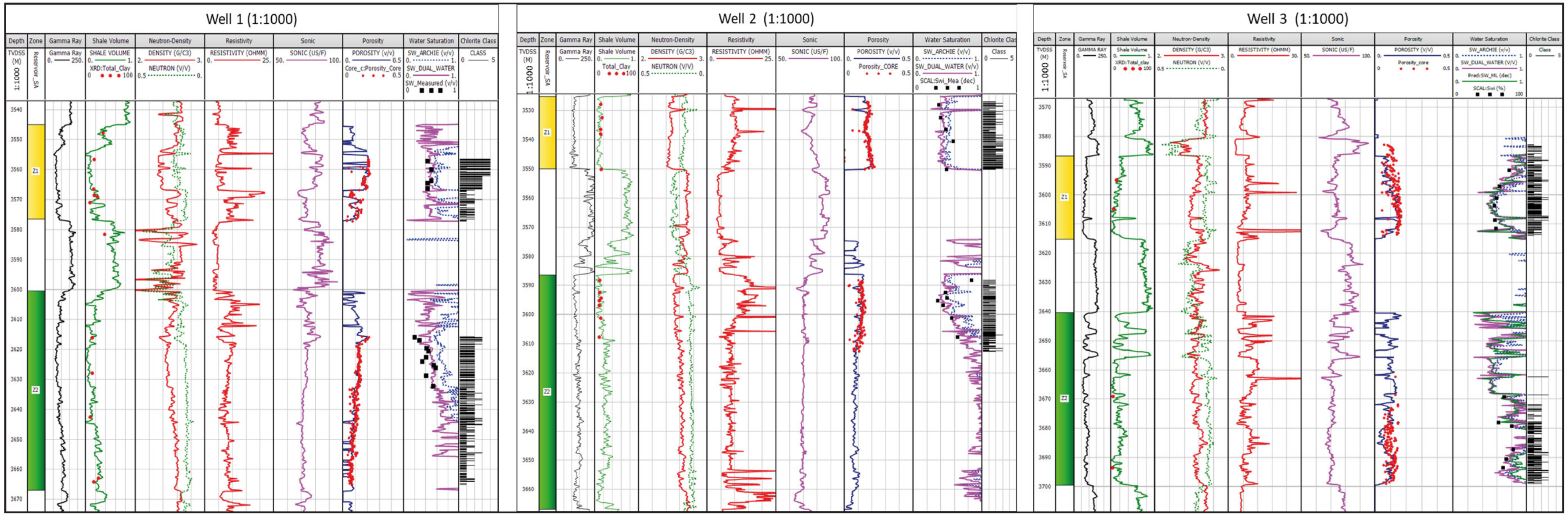

Figure 9. Representative well logs, core analysis data, and calculated porosity and water saturation for variably chlorite-cemented Z1 and Z2 reservoirs in Wells 1, 2, and 3 of The SA Field. High-porosity intervals in Class 3 and Class 4 at depths of approximately 3560 and 3620 mTVDSS in Well 1 are characterized by high neutron, low density, high sonic, and low resistivity responses. Track 9 shows water saturation estimated using the Dual-Water model, which exhibits better agreement with core data than the Archie model in Well 3, calculated and ML-predicted water saturation are additionally compared.

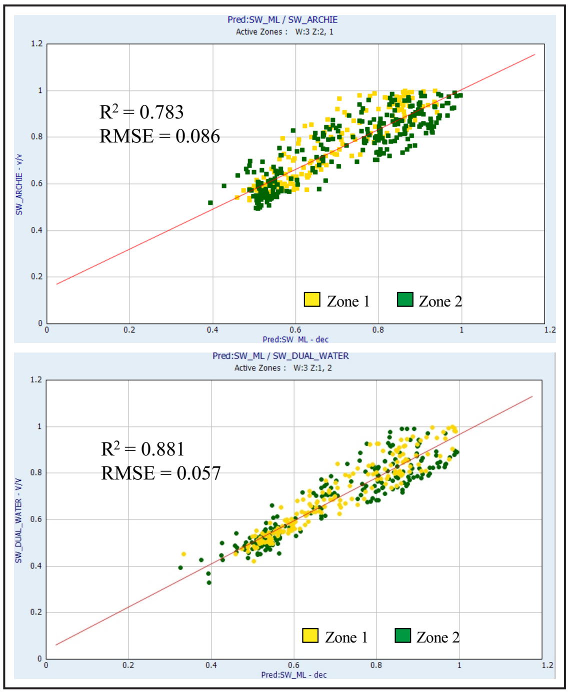

Figure 10. Demonstrates the coefficient of determination (R^2) between ML-predicted water saturation and Sw calculated by Archie (a) and Dual-Water (b) models.

Table 2. Water Saturation Prediction Using ML and Comparison with Archie and Dual-Water models The Table Summarizes Standard Deviation (SD), Root Mean Squared Error (RMSE), and Coefficient of Determination (R^2) Between Predicted and Calculated Sw

Approaches	Min	Max	SD	RMSE	R^2
Archie	0.357	1	0.167	0.086	0.783
Dual - Water	0.275	1	0.192	0.057	0.881
ML	0.274	1	0.185	-	-

mineralogical differences are consistent with previous studies indicating that litharenitic and feldspathic litharenitic sandstones derived from low-grade metamorphic sources are prone to chlorite development during early diagenesis (Peng *et al.*, 2009).

Diagenetic features observed in the Z1 and Z2 sandstone reservoir (Figure 11) include compaction, feldspar and lithic grain dissolution, carbonate cementation, quartz overgrowth, and authigenic clay mineralization. The cements are quartz, carbonate such as siderite and dolomite (Figures 12a, c), and clays such as illite and chlorite in Figure 6, Figure 12, and Figure 13. Quartz and chlorites are the most characteristic cement types in sandstone reservoirs of SA Field.

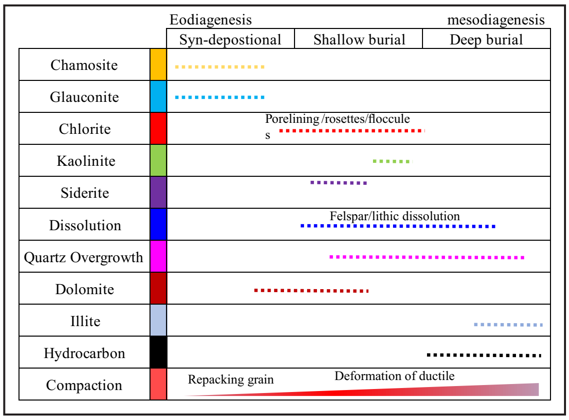

Figure 11. Diagenetic sequence of the studied Z1 and Z2 reservoirs in SA Field.

Compaction and quartz overgrowth form the main porosity-destructive phases that dominate the diagenetic overprint. Sandstones were moderately to strongly compacted with mainly point-line grain contacts and line contacts (Figure 6d). With increasing burial depth, compaction of labiles becomes progressively more important, with ductile grains being deformed and squashed through pore throats, resulting in diminishing porosity and permeability. Quartz overgrowths also become increasingly more developed but appear to have been partly inhibited by the high lithic content of the sediment (Figure 6c). The highest levels of quartz overgrowth are in Z2 of this well. It is possible that the lower quartz overgrowth levels in Z1 are attributable to the decreasing development of chlorite and the retarding effects of oil migration on later overgrowth formation, which is illustrated by a heavy residual oil in Figure 13d at the base of the Z1 reservoir.

Overall, chlorite exerts a dual control on reservoir quality in The SA Field. Early development of grain-coating chlorite pellicles plays a positive role by inhibiting quartz overgrowth and preserving intergranular porosity, as evidenced by continuous pore-lining chlorite rims observed under SEM (Figures 12b, e) and thin section (Figures 13c, e), particularly in Class 3 where permeability reaches its optimum (Figures 6b-d, 11). However, progressive formation

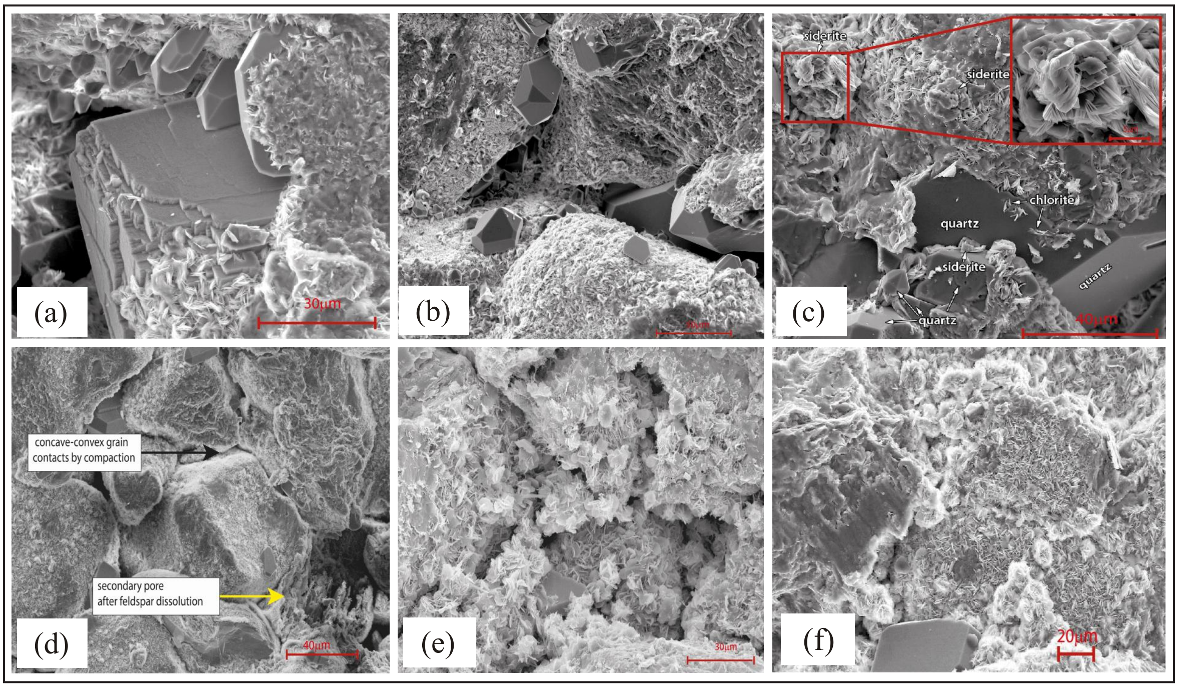

Figure 12. Typical features in SA Field by SEM. (a) Finely stepped dolomite formed around incipient quartz overgrowths and earlier grain-coating chlorite. (b) Typical intergranular pore system, lined by early authigenic chlorite. Well-developed chlorite occurs as rosetted boxwork platelets. (c) Well developed quartz overgrowth occluding an intergranular pore. A siderite crystal has been enclosed by the quartz. The red box shows the siderite crystals intergrown with the chlorite. (d) The secondary pore (arrow) is after feldspar dissolution. A fine grained moderately sorted sandstone with dominant long to locally concave-convex grain contacts. (e) Authigenic chlorite is an early pore lining phase occurring as boxwork platelets and rosette aggregates. They inhibit quartz overgrowth when continuous but also constrict pore throats. The high surface area increases microporosity and SW. (f) Chlorite 'granules' are widespread, commonly blocking pore throats. Grain contact faces are commonly coated by compacted chloritic clays. Most of the grain-coating chlorite is oriented normal or near-normal to the grain surface.

and migration of chlorite floccules and rosette morphologies into pore throats leads to partial or complete pore-throat blockage, as shown by abundant chlorite granules and rosette aggregates plugging pore spaces in SEM images (Figure 12f) and thin sections (Figure 13d), causing significant permeability reduction despite relatively high porosity, as observed in Class 4 (Figures 6e, 12–13). This indicates that the diagenetic transition from pore-lining to pore-filling chlorite represents a critical threshold beyond which chlorite becomes detrimental to reservoir flow capacity.

Chlorite in The SA Field is interpreted to form predominantly during early diagenesis under mixed fluvial–marine pore-water conditions (Hillier, 1994), with its spatial development influenced by the relative position to river mouths and regressive-transgressive delta stacking patterns that control early sediment flushing history. The occurrence of glauconite and chamosite in thin sections (Figure 13a) is consistent with marginal marine depositional environments (Brindley *et al.*, 1951; Sylvestre *et al.*, 2017), indicating increased marine influence during sedimentation. The presence of carbonaceous material and phosphatic bone fragments (Figure 13b) further suggests intrabasinal reworking within a marginal marine setting. With increasing burial depth, clay mineral transformations become a major source of chlorite during diagenesis.

Smectite and kaolinite are known to transform into chlorite under high pH and Fe-rich conditions (Chen *et al.*, 2011), with the kaolinite–chlorite conversion primarily controlled by burial depth and temperature (Moraes and De Ros, 1992). Boles and Franks (1979) revealed that this process typically appeared at a depth of 3,500 to 4,500 m. Given that the studied reservoirs are deeper

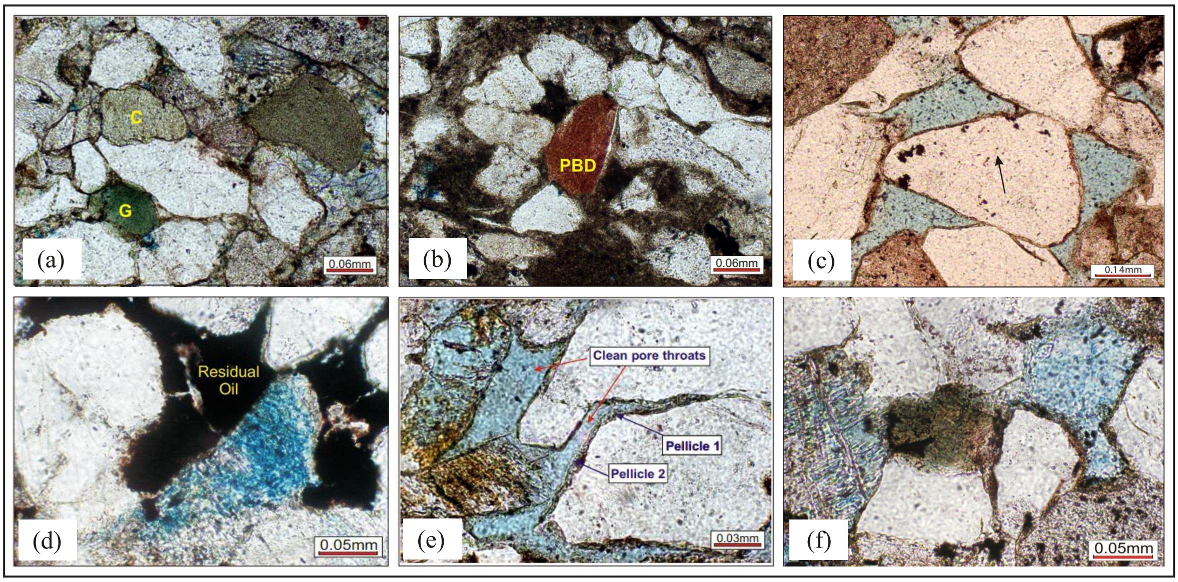

Figure 13. Typical features in SA Field by optical photomicrographs (thin section); (a) Glauconite (G) and chamosite (C) occur mostly as traces indicating increased marine influence; (b) Phosphatic bone debris (PBD) observed in traces are associated with occasional common intraclasts and more abundant bioclasts, suggesting a moderate degree of intrabasinal reworking; (c) Intergranular pores have been preserved locally by continuous grain coating chlorite; (d) Mat-like residual oil forms an intergranular pore-plugging phase; (e). Clean pore throats without chlorite floccules and rosettes, resulting in good permeability and porosity; (f) Framework grain dissolution of feldspars, some lithics and chamosite has enhanced the pore systems with honeycomb feldspar (left) and an oversize pore (right).

than 3,500 m, and XRD analysis shows no detectable kaolinite, chlorite is therefore interpreted as largely authigenic. SEM observations reveal widespread early pore-lining chlorite occurring as rosetted boxwork platelets (4-8 µm; Figures 12b-c), which increase microporosity and irreducible water saturation while reducing net permeability, particularly in finer-grained samples (Xia *et al.*, 2020). This interpretation is supported by SCAL results showing a strong negative correlation between water saturation and permeability (R = 0.76; Figure 14), indicating that chlorite-related microporosity generates large internal surface area and high proportions of immobile bound water, leading to elevated Sw and reduced flow capacity.

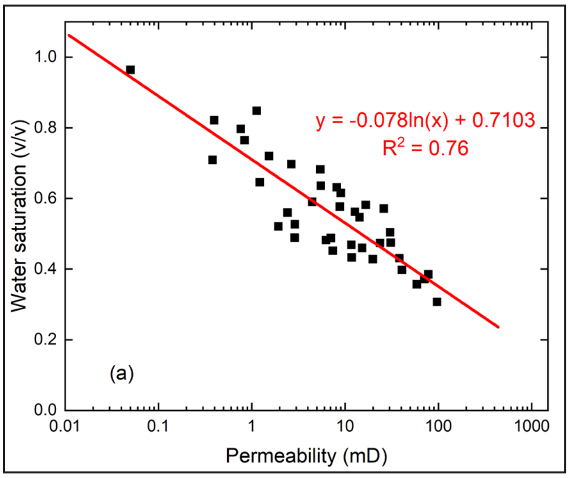

Figure 14. Relationships between irreducible water saturation and permeability for SA Field.

Effects of Chlorite on Well-log Responses And Petrophysical Interpretation

Chlorite exerts a systematic control on well-log responses and petrophysical interpretation in the Z1 and Z2 reservoirs of The SA Field. Gamma ray logs show limited sensitivity to chlorite because this mineral does not contain radioactive elements (Worden *et al.*, 2020). In contrast, density, neutron, sonic, and resistivity logs display consistent and diagnostic responses to increasing chlorite content. In chlorite-rich intervals (Classes 3 and 4), bulk density decreases (<2.42 g/cm³) and sonic transit time increases due to enhanced porosity preserved by the inhibition of quartz overgrowth (Anjos *et al.*, 1999).

Neutron responses are elevated as a result of both increased porosity and the high hydrogen content associated with chlorite crystal structures and bound water (Rider, 2002). Chlorite-bearing sandstones also exhibit low resistivity signatures, reflecting increased surface conductivity and high irreducible water saturation linked to chlorite microporous texture and cation exchange capacity (Durand *et al.*, 2000; Hamada and Al-Awad, 2000 ; Si *et al.*, 2022). These effects lead to systematic overestimation of water saturation when applying Archie's equation, which assumes clean sand conditions and neglects bound water conductivity (Clavier *et al.*, 2003). In contrast, the Dual-Water model better reproduces core-measured water saturation in chlorite-rich intervals by explicitly accounting for both bound and free water phases, particularly in reservoirs characterized by interbedded sandstones and claystones of The Lower Miocene Z1 and Z2 formations (Duyen *et al.*, 2023; Tuan *et al.*, 2016). The presence of rosetted and boxwork chlorite textures further enhances microporosity and irreducible water saturation, reinforcing the necessity of mineralogically informed petrophysical models in these reservoirs (Xia *et al.*, 2020).

Machine Learning Model for Sw in Context of Chlorite Impaction

Chlorite-rich reservoirs present significant challenges for accurate water saturation determination, as traditional methods like Archie often overestimate Sw due to chlorite's high bound water content and influence on electrical properties. To overcome these limitations, this study prioritized the use of validated available input data for machine learning-based Sw prediction. The workflow began with detailed characterization of reservoir petrophysical properties and careful selection of an Sw interpretation model suitable for chlorite-bearing sandstones to ensure reliable training labels. The regression-based ML models were trained using petrophysical log data and core-calibrated Sw from Well 1 and Well 2, with the dataset randomly split into 80 % for training, and 20 % for testing to evaluate model generalization.

In this study, water saturation prediction was formulated as a regression problem, and the performance of a tree-based boosting algorithm, LightGBM (LGBM) was evaluated and applied. Model training was conducted using cross-validation to ensure objective performance assessment, followed by evaluation on an independent test set. The models exhibited stable and robust performance, with test R^2 values approaching 0.94 and low prediction errors (MSE ~ 0.002; RMSE ~ 0.04), indicating high accuracy and consistency. Based on these results, the optimal model was subsequently applied to Well 3 as an independent blind test.

In Well 3, the predicted water saturation closely matches with both Dual-Water-derived Sw and the Archie-based Sw (Track 9 of Figure 9 in Well 3), indicating a limited chlorite influence in this well. This result is consistent with core descriptions, thin-section petrography, SEM observations, and well-log responses, which collectively indicate a lower abundance of chlorite compared to Well 1 and Well 2, as discussed in previous sections. The convergence of ML-predicted Sw with Archie-derived Sw in Well 3 therefore provides an independent validation that the reservoir interval is weakly affected by chlorite. In contrast, in chlorite-rich intervals (*e.g.* Well 1), the ML-predicted Sw shall align more closely with the Dual-Water model and diverge significantly from the Archie-derived Sw. These results demonstrate that the ML model not only predicts Sw accurately, but also implicitly captures the chlorite-related controls on petrophysical behaviour.

Based on this observation, the proposed ML workflow can be extended as a diagnostic tool by applying the trained model to additional wells across The SA Field. By comparing ML-predicted Sw with Archie-derived Sw in a larger well dataset (approximately 31 wells without core data), the spatial distribution and relative intensity of chlorite influence can be inferred. This provides a practical and cost-effective approach for mapping chlorite impact at the field scale, and supports future studies aimed at integrating ML-based Sw prediction with diagenetic and reservoir properties evaluation.

Conclusions

Authigenic chlorite is the primary clay phase in the sandstone reservoirs of SA Field. The chlorite effect increases towards the upper sections of both Zone 1 and Zone 2, and declines gradually from north to south of this field. As a grain-coating mineral, chlorite plays a crucial role in preserving porosity in deeply buried sandstones by inhibiting quartz cementation on detrital quartz grain surfaces in this area. However, chlorite floccules present within the pore throats significantly reduce permeability, despite the relatively high porosity observed in these formations. Pore lining with rosetted boxwork chlorite in the SA Field causes the increasing of Sw and decreasing of permeability.

The occurrence of chlorite in reservoirs is distinctly identifiable in well logs due to its high neutron, high sonic, and high-density log responses. Furthermore, chlorite-rich sandstones exhibit high residual water saturation, leading to abnormally low resistivity readings in oil-filled intervals, potentially complicating hydrocarbon identification.

Hydrocarbon saturation estimation using the clean sand Archie's equation indicates higher water saturation in this SA Field with high chlorite content. Meanwhile, the shaly-sand Dual-Water model provides a more accurate interpretation in chlorite-affected intervals, as confirmed by core analysis results. This suggests that the Dual-Water model better accounts for the influence of chlorite on electrical resistivity, leading to improved hydrocarbon saturation estimation in these formations.

The state-of-the-art LightGBM-based machine learning model, integrating petrophysical well logs and core data, enables accurate prediction of water saturation in chlorite-rich reservoirs. The ML-predicted Sw values closely match those derived from the Dual-Water model, and are validated by core plug measurements. Importantly, the consistency between ML-predicted Sw and Archie-derived Sw in wells with low chlorite influence demonstrates that the model can also be applied as a diagnostic tool to infer chlorite impact in areas lacking core data or with limited well-log suites.

Acknowledgements

The authors would like to sincerely thank Petrovietnam and the Vietnam Petroleum Institute for providing and allowing us to publish them. Furthermore, we appreciate the input by editors and reviewers and the respected editor for constructive comments that significantly improved this manuscript.

References

Anjos, S.M.C., De Ros, L.F., and Silva, C.M.A., 1999. Chlorite Authigenesis and Porosity Preservation in the Upper Cretaceous Marine Sandstones of the Santos Basin, Offshore Eastern Brazil. *In*: *Clay Mineral Cements in Sandstones*, p.289-316. DOI: 10.1002/9781444304336.ch13.

Archie, G.E., 2003. The Electrical Resistivity Log as an Aid in Determining Some Reservoir Characteristics. *SPE Reprint Series*, (55), p.9-16. DOI: 10.2118/942054-g.

Asquith and Gibson, 1982. *Basic Well Log Analysis for Geologists*. AAPG, 234pp.

Boles, J.R. and Franks, S.G., 1979. Clay diagenesis in Wilcox sandstones of Southwest Texas: implications of smectite diagenesis on sandstone cementation. *Journal of Sedimentary Research*, 49 (1), p.55-70. DOI:10.1306/212F76BC-2B24-11D7-8648000102C1865D.

Brindley, G.W., Dunham, K.C., Eyles, V.A., and Taylor, J.H., 1951. The crystal structure of some chamosite minerals (With Plate XII). *Mineralogical Magazine and Journal of the Mineralogical Society*, 29 (212), p.502-525. DOI:10.1180/minmag.1951.029.212.04.

Brooks, R.H. and Corey, A.T., 1964. Hydraulic Properties of Porous Media, *Hydrology Paper,* 3.

Bukar, I., Adamu, M.B. and Hassan, U., 2019. A machine learning approach to shear sonic log prediction. *Society of Petroleum Engineers - SPE Nigeria Annual International Conference and Exhibition 2019, NAIC 2019*, (8), p.5-7. DOI:10.2118/198764-MS.

Chen, G., Du, G., Zhang, G., Wang, Q., Lv, C., and Chen, J., 2011. Chlorite cement and its effect on the reservoir quality of sandstones from the Panyu low-uplift, Pearl River Mouth Basin. *Petroleum Science*, 8 (2), p.143-150. DOI: 10.1007/s12182-011-0127-z.

Clavier, C., Coates, G., and Dumanoir, J., 2003. Theoretical and Experimental Bases for the Dual-Water Model for Interpretation of Shaly Sands. *SPE Reprint Series*, (55), p.153-168.

Deer, W.A., Howie, R.A., and Zussman, J., 2013. An Introduction to the Rock-Forming Minerals. DOI:10.1180/DHZ.

Durand, C., Cerepi, A., and Brosse, E., 2000. Effect of Pore-Lining Chlorite on Petrophysical Properties of Low-Resistivity Sandstone Reservoir.

Duyen, P.T., Hoa, T.T., Dam, M.H., and Tham, N.T., 2023. Stratigraphic Significance of Larger Benthic Foraminifera in Miocene Carbonates from Nam Con Son Basin, Vietnam. *Stratigraphy and Geological Correlation*, 31 (6), p.676-699. DOI:10.1134/S0869593823060035.

Folk, R.L., 1974. *Petrology of Sedimentary Rocks*. Hemphill Publishing Co., Austin, 170pp.

Friedman, J.H., 2001. Greedy function approximation: A gradient boosting machine. *Annals of Statistics*, 29 (5), p.1189-1232. DOI: 10.1214/aos/1013203451.

Fyhn, M.B.W., Boldreel, L.O. and Nielsen, L.H., 2009. Geological development of the Central and South Vietnamese margin: Implications for the establishment of the South China Sea, Indochinese escape tectonics and Cenozoic volcanism. *Tectonophysics*, *478 (3-4)*, p.184-214. DOI:10.1016/j.tecto.2009.08.002.

Gingele, F.X., De Deckker, P., and Hillenbrand, C.D., 2001. Clay mineral distribution in surface sediments between Indonesia and NW Australia - Source and transport by ocean currents. *Marine Geology*, 179 (3-4), p.135-146. DOI:10.1016/S0025-3227(01)00194-3.

Hadavimoghaddam, F., Ostadhassan, M., Sadri, M.A., Bondarenko, T., Chebyshev, I., and Semnani, A., 2021. Prediction of water saturation from well log data by machine learning algorithms: Boosting and super learner. *Journal of Marine Science and Engineering*, 9 (6), 666. DOI:10.3390/jmse9060666.

Hall, R. and Spakman, W., 2015. Mantle structure and tectonic history of SE Asia. *Tectonophysics*, 658, p.14-45. DOI:10.1016/j.tecto.2015.07.003.

Hamada, G.M. and Al-Awad, M.N.J., 2000. Technical note: Petrophysical evaluation of low resistivity sandstone reservoirs. *Journal of Canadian Petroleum Technology*, 39 (7), p.7-14.

Hillier, S., 1994. Pore-lining chlorites in siliciclastic reservoir sandstones: electron microprobe, SEM and XRD data, and implications for their origin. *Clay Minerals*, 29 (4), p.665-679. DOI:10.1180/claymin.1994.029.4.20.

Hu, K., Liu, X., Chen, Z., and Grasby, S.E., 2023. Mineralogical Characterization From Geophysical Well Logs Using a Machine Learning Approach: Case Study for the Horn River Basin, Canada. *Earth and Space Science*, 10, p.1-21. e2023EA003084. https://doi.org/10.1029/2023EA003084

Jia, Y., Cao, Y., Lin, C. and Wang, J., 2018. Diagenetic evolution and its implication for reservoir quality: a case study from the Eocene Es4 interval, Dongying Depression, Bohai Bay Basin, China. *Geosciences Journal*, 22 (1), p.91-103. DOI:10.1007/s12303-017-0029-1.

King, H., 2019. *Chlorite*. https://geology.com/minerals/chlorite.shtml.

Leverett, M.C., 1941. Capillary Behavior in Porous Solids. *Journal fur die Reine und Angewandte Mathematik*, 195 (200), p.129-139. DOI: 10.1515/crll.1958.200.129.

Li, K., Xi, K., Cao, Y., Niu, X., Wu, S., Feng, S. and You, Y., 2021. Chlorite authigenesis and its impact on reservoir quality in tight sandstone reservoirs of the Triassic Yanchang formation, southwestern Ordos basin, China. *Journal of Petroleum Science and Engineering*, 205, p.108843. DOI:10.1016/j.petrol.2021.108843.

Machado, M.R., Karray, S. and De Sousa, I.T., 2017. LightGBM: A Highly Efficient Gradient Boosting Decision Tree. *14th International Conference on Computer Science and Education, ICCSE 2019*, (Nips), p.1111-1116. DOI: 10.1109/ICCSE.2019.8845529.

Mazumder, R., 2016. *Sediment provenance: Influences on compositional change from source to sink*. Elsevier B.V, 614pp.

Mollajan, A. and Memarian, H., 2013. Estimation of water saturation from petrophysical logs using radial basis function neural network. *Journal of Tethys*, 1 (2), p.156-163.

Moraes, M. and De Ros, L., 1992. Depositional, Infiltrated and Authigenic Clays in Fluvial Sandstones of the Jurassic Sergi Formation, Recôncavo Basin, northeastern Brazil. *In*: *SEPM Special Publication*, p.197-208. DOI: 10.2110/pec.92.47.0197.

Peng, J., Liu, Jinku, Wang, Y. and Liu, Jianfeng, 2009. Origin and controlling factors of chlorite coatings-an example from the reservoir of T3x Group of the Baojie area, Sichuan Basin, China. *Petroleum Science*, 6 (4), p.376-382. DOI:10.1007/s12182-009-0057-1.

Rider, M., 2002. *The Geological Interpretation of Well Logs*. Sutherland : Rider-French Consulting, 280pp.

Saumya, S., Naqeeb, I., Vij, J., Khambra, I. and Kumar, A., 2019. Saturation forecast using machine learning: Enabling smarter decision-making capabilities. *Society of Petroleum Engineers - Abu Dhabi International Petroleum Exhibition and Conference 2019, ADIP 2019* [Preprint]. DOI:10.2118/197419-ms.

Shao, W., Chen, S., Eid, M. and Hursan, G., 2019. Carbonate Log Interpretation Models Based On Machine Learning Techniques. *In*: DOI: 10.30632/T60ALS-2019_SSS.

Si, Z., Chen, J. and Peng, H., 2022. Investigation on mechanism of low-resistivity oil reservoir in Minghuazhen and Guantao Formation of Nanpu Sag. *Petroleum Research* [Preprint]. DOI: 10.1016/j.ptlrs.2022.05.004.

Sylvestre, G., Evine Laure, N.T., Gus Djibril, K.N., Arlette, D.S., Cyriel, M., Timoléon, N. and Jean Paul, N., 2017. A mixed seawater and hydrothermal origin of superior-type banded iron formation (BIF)-hosted Kouambo iron deposit, Palaeoproterozoic Nyong series, Southwestern Cameroon: Constraints from petrography and geochemistry. *Ore Geology Reviews*, 80, p.860-875. DOI:10.1016/j.oregeorev.2016.08.021.

Tiab, D. and Donaldson, E.C., 2015. *Petrophysics: Theory and Practice of Measuring Reservoir Rock and Fluid Transport Properties*. Gulf Professional Publishing.

Tuan, N.Q., Tung, N.T., and Van Tri, T. V., 2016. Seismic interpretation of the Nam Con Son Basin and its Implication for the tectonic evolution. *Indonesian Journal on Geoscience*, 3 (2), p.127-137. DOI:10.17014/ijog.3.2.127-137.

Tung, N.T., 2015. Tectonic Development of Nam Con Son basin Based on New Seismic Data Interpretation, in *AAPG Asia Pacific Geoscience Technology Workshop (GTW) Tectonic Evolution and Sedimentation of South China Sea Region*. http://www.searchanddiscovery.com/abstracts/pdf/2015/90236apr/abstracts/ndx_tung.pdf.

Worden, R.H., Griffiths, J., Wooldridge, L.J., Utley, J.E.P., Lawan, A.Y., Muhammed, D.D., Simon, N. and Armitage, P.J., 2020. Chlorite in sandstones. *Earth-Science Reviews*, 204, p.103105. DOI:10.1016/j.earscirev.2020.103105.

Xia, H., Perez, E.H. and Dunn, T.L., 2020. The impact of grain-coating chlorite on the effective porosity of sandstones. *Marine and Petroleum Geology*, 115, p.104237. DOI: 10.1016/j.marpetgeo.2020.104237.